American Mineralogist, Volume 87, pages 1390–1400, 2002

Temperatures from triple-junction angles in sulfides

JOHN LUSK,* BRIAN O. E. CALDER, AND TERENCE E. FREEMAN

Department of Physics, Macquarie University, N.S.W., 2109, Australia

ABSTRACT

Experiments carried out between 280 and 980 °C demonstrate that dihedral angles for galena, θ_{gn}, in sphalerite-galena-sphalerite triple-junctions decrease with increasing temperature, and that the rate of change increases in the same direction. Similar behavior is evident for sphalerite, θ_{sp}, in galena-sphalerite-galena triple-junctions, and also for pyrrhotite, θ_{po}, in sphalerite-pyrrhotite-sphalerite triple-junctions. Triple-junction thermometry (TJT) is therefore most sensitive at high to very high temperatures where isotope thermometers are least sensitive. The method relies on the temperature-dependence of competitive surface tensions between shared surfaces of intergrown minerals. Because chemical interaction is not a prerequisite, the TJT method is potentially applicable to a variety of mineral pairs found in regional metamorphic situations. The method requires a slightly modified microscope equipped with a precision X-Y stage.

The application of θ_{gn}-*T* (temperature) and θ_{po}-*T* calibrations to regionally metamorphosed sulfide ores yields temperatures that compare reasonably with temperatures obtained from sulfur isotopes and other geothermometers. Maximum regional metamorphic temperatures of ~470–480, ~590, and ~700 °C were obtained for the Bathurst (New Brunswick = greenschist facies), Ruttan (Manitoba = amphibolite facies) and Broken Hill (N.S.W. = granulite facies) deposits, respectively. The θ_{gn} and θ_{po} thermometers also reveal recrystallization effects in microfabrics.

INTRODUCTION

Some of the world's largest Pb-Zn sulfide deposits have been regionally metamorphosed at temperatures between 300 and 800 °C and at pressures up to 8 kbars. An improved understanding of the effects of metamorphism on sulfide deposits is advantageous because the maximum temperature of metamorphism determines mean grain size and the grain shapes of minerals. These factors are of significance because they affect the efficiency of mineral separation in sulfide ores. A thorough knowledge of sulfide ore microfabrics is valuable to sulfide petrologists seeking a better understanding of metamorphic temperatures (*T*) and pressures (*P*), as well as metamorphic histories.

Chemically based mineralogical thermometers have long been applied to regionally metamorphosed sulfide deposits and their enclosing rocks. These thermometers have led to broad agreement on respective *T-P* conditions for the various grades of regional metamorphism. Among the thermometers used, sulfur (Ohmoto 1986) and oxygen (Valley 1986) isotope thermometers have been extremely important due to their pressure-independence and their application over wide temperature ranges. For sulfide ores, the sphalerite-galena sulfur isotope thermometer has been applied extensively (Ohmoto 1986). Fluid inclusion thermometry is commonly useful at lower grades of metamorphism where aqueous fluids are typically present (Roedder 1986). Very precise temperatures can be obtained directly in situations where fluid boiling is evident, but pressure corrections must be applied to homogenization temperatures obtained from other situations (Roedder 1986). The arsenopyrite thermometer has received limited attention, but has been applied successfully to some sulfide deposits (e.g., Sharp et al. 1985).

The world's Pb and Zn are obtained from the common sulfides galena (PbS) and sphalerite (ZnS) that occur together in multi-million ton deposits in the crust of continents. Predominant among these are sedimentary sulfide deposits of widely variable age that have been buried and heated in the crust for millions of years. Stanton (1964) has demonstrated that sulfide microfabrics in regionally metamorphosed sulfide deposits have resulted from surface tension-induced grain growth in response to increases in temperature. Depending on local geothermal gradients, extreme depths of burial to around 25–30 km equate with maximum regional metamorphic temperatures of between ~600 and ~800 °C. The highest metamorphic temperatures promote the highest diffusion rates and generate the coarsest mean grain sizes. Stresses in the Earth's crust cause a variety of deformation effects that can be large scale, such as in folding, or localized within microfabrics. Sulfide deposits are characteristically affected to varying degrees during long periods of slow cooling from maximum metamorphic temperatures. Localized deformation generates lattice strain within minerals, and temperature simultaneously relieves strain through annealing and recrystallization at prevailing temperatures. Consequently, ongoing or multiple deformation events during cooling can yield a range of recrystallization temperatures within a given deposit (Lusk and Krouse 1997).

In the absence of fluid-filled cavities, solid grains share contact surfaces with adjacent grains. Where the grains are of

* E-mail: luskjoru@bigpond.com.au

the same mineral, classic "foam" structures of polygonal and equant grains are produced that have true triple-junction angles of 120 degrees (Smith 1950). However where grains are of different minerals, then relative differences in surface tensions determine angular relationships between shared surfaces, and hence overall grains shapes (Stanton 1964). Large differences may allow some minerals to develop crystal surfaces with others molding around them, as is observed for pyrite (FeS_2) and arsenopyrite (FeAsS) contained in a sphalerite-galena matrix. However, where sphalerite and galena occur together as trapped inclusions in pyrite porphyroblasts, genuine pyrite-galena-sphalerite triple-junctions can be observed. Figure 1a reveals that dihedral angles for pyrite are less than 180 degrees in these situations, thus explaining why pyrite porphyroblasts contained in galena-sphalerite assemblages commonly exhibit rounded embayments and partly curved outer surfaces. Figure 1b contrasts the smaller dihedral angles for galena and pyrrhotite that were investigated in the present study.

The principles governing grain shape morphology, surface tension interactions, grain boundary migration, and annealing and recrystallization were established some fifty years ago by metallurgists in their study of metals and alloys (Smith 1964). Stanton and Gorman (1968, 1970) later demonstrated that these principles apply also to sulfides in Pb-Zn ores. Importantly, Stanton and Gorman (1968) reported a broad temperature-dependence of the dihedral angle for galena, θ_{gn}, in sphalerite-galena-sphalerite triple-junctions in experiments at temperatures between 300 and 1000 °C. However, difficulties were encountered with the natural samples used in these experiments and resulted in an unacceptable degree of scatter in the data obtained at intermediate and higher temperatures. It is surprising that this promising research was abandoned and has not been revisited until now.

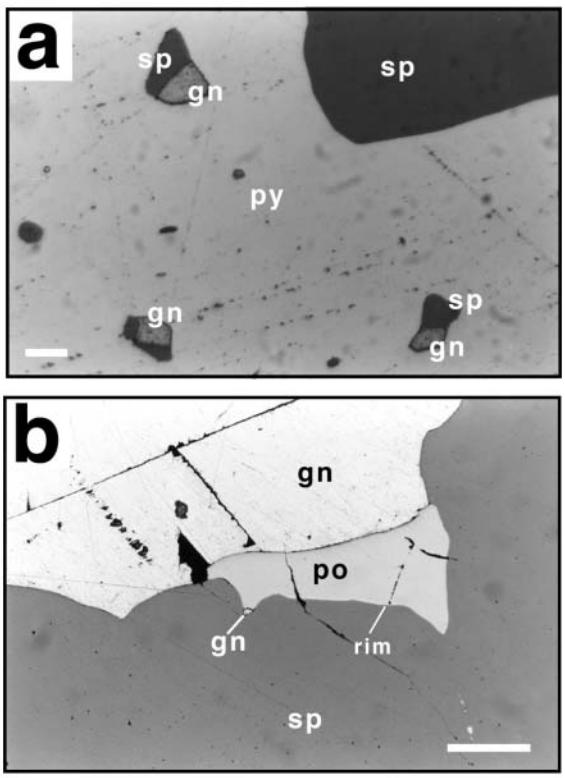

FIGURE 1. Photomicrographs of (**a**) three sphalerite–galena (sp–gn) inclusions in a pyrite (py) porphyroblast of the SWBD sample. The scale bar represents 10 micrometers. (**b**) Dihedral angles for galena (gn) and pyrrhotite (po) in sphalerite (sp) of the Broken Hill no. 4 sample. The scale bar represents 100 micrometers.

METHODS

Materials and experiments

Natural samples together with pellets made from synthetic sphalerite-galena mixtures were used in the calibration experiments. The natural samples comprised cylinders 8 mm in diameter and 10 mm long that were prepared from a single sample of fine-grained and foliated Cobar ore (C.S.A. Mine, N.S.W.) showing an annealed micro fabric. Sulfides constitute >95% of the modal mineralogy in this ore. The major sulfides include sphalerite (~50 vol% with FeS content of ~20 mol%) and galena (~30 vol%), and the minor sulfides comprise pyrrhotite (~10 vol%) and chalcopyrite (~5 vol%).

Due to experimental failures with natural samples above 680 °C, it was found necessary to use synthetic pellets at the highest temperatures. Compressed pellets 5 mm in diameter and 6–8 mm long were prepared with core mixtures of ~40% reagent PbS powder and ~60% of 200–325 mesh Broken Hill (N.S.W.) sphalerite (~35 mol% FeS) concentrate surrounded by envelopes of PbS powder to prevent crumbling.

The Cobar ore samples and compressed pellets were heated in evacuated Vycor glass capsules at temperatures from 280 to 980 °C for periods ranging from 375 to 4 days, respectively. The capsules were heated in the hot spots of tube furnaces and controlled to within ± 5 °C over the duration of the experiments.

Equipment

A customized Leitz Orthoplan microscope equipped with 10× eyepieces and a 100× NPL air objective was used for measurement of dihedral angles. The essential elements of the customization are discussed below and illustrated in Figure 2.

A Perspex disk with a goniometer scale (0.5 degree divisions) was clamped to the microscope tube containing one of the 10× eyepieces (Fig. 2a). A machined brass ring containing a pointer blade for reading angles on the goniometer scale was clamped to the free end of the rotating eyepiece that contains cross-hairs and a graticule. A smear of lubricant applied to the outer surface of the measuring eyepiece ensures smooth rotation and sensitive angular adjustments at the working magnification.

The rotating stage of the microscope is lowered to its maximum position and firmly clamped prior to fitting a customized X-Y stage from a dedicated Leitz microhardness tester as shown in Figure 2b. The latter is fitted with a pair of digital readout micrometers with 25 mm of travel, adjustable zeroing, and 1 micron resolution. Aluminum sample plates or a machined brass guide plate can be located and firmly screwed in position on the top of the X-Y stage using a pair of machine screws.

The experimental run products were mounted in resin contained within the bores of 12 mm thick brass holders (25 mm

diameter) with three vertical flats at right angles. This arrangement enables the brass sample blocks and a matching indented location block to be held in position firmly (with a locking screw) on a brass guide plate that is screw-mounted on the X-Y stage. When used in conjunction with the location block (allowing re-setting of zeros in X-Y space), the sample holders can be removed readily and relocated accurately in X-Y space on the microscope stage. Unheated ore samples were typically prepared as thick plates (~30 mm × ~20 mm × ~8 mm) and polished on one side. The latter were supported with plasticine on the 5 mm thick sample plates and the polished surfaces leveled with a Leitz leveling press.

Measurement of dihedral angles

Where a sufficiently large number of dihedral angles are measured, the most frequently occurring angle should represent the true dihedral angle, that is, where the line of triple-junction intersection is perpendicular to the polished surface (Smith 1964). The present authors used a model to confirm this assertion. Our model selects a plane of random orientation and calculates the dihedral angle formed as this plane intersects a triple junction of fixed orientation. This model can be used to predict the accumulated distribution profile of apparent and true angles, for any number of trials, that relate to a chosen true angle. Figure 3 shows: 680 °C experimental data for which iterative analysis suggests a mode at 89 ± 2 degrees (Fig. 3c); data generated by running the model for the same number of trials (Fig. 3b); and finally, a very large number of trials in order to smooth out statistical variations (Fig. 3a). For this type of model there is no convenient formula that enables us to construct a smooth curve as shown in Figure 3a. Indeed, this modeling would be of little value because of the considerable statistical fluctuations that are so obvious in Figures 3b and 3c. Our study shows that for dihedral angles well away from 90 degrees the top of a background bell-shaped curve does not coincide exactly with the cusp that indicates the true dihedral angle. This offset occurs because of the skewed nature of these curves. We therefore do not recommend the fitting of broad statistical curves such as the Gausian distribution.

It is impractical to measure very large numbers of dihedral angles, although larger numbers of measurements obviously yield increasingly reliable results. It is therefore necessary to estimate the smallest number of measurements that will yield reliable results. For 1000 measurements, the most frequent angle

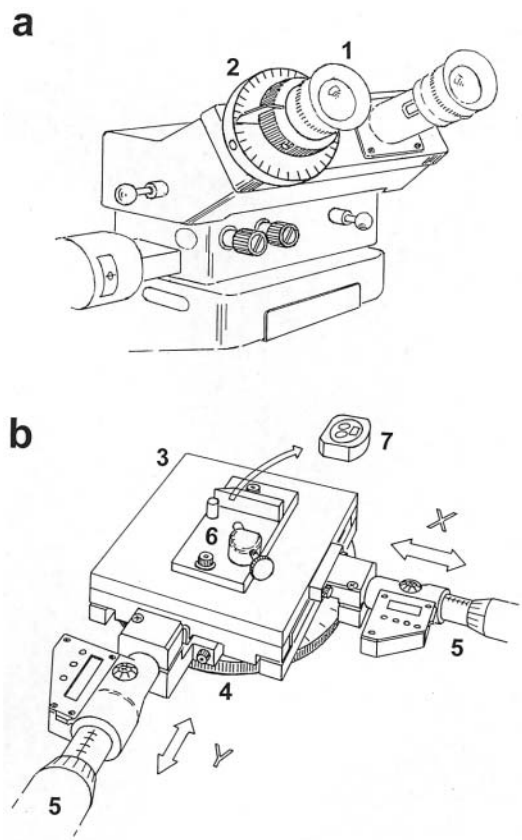

FIGURE 2. Sketch of parts for a Leitz Orthoplan microscope. (**a**) binocular head showing rotatable Periplan 10× occular with indicator blade (1) and the goniometer disk (2) fixed to one occular tube; (**b**) modified Leitz X-Y stage (3) mounted on the microscope stage (4). Digital micrometers (5), a sample location plate (6), and an interchangable sample block (7) are also indicated.

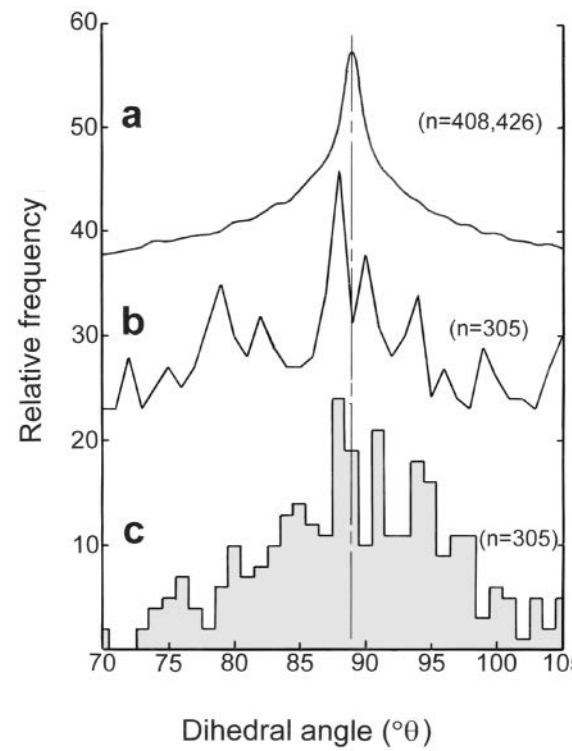

FIGURE 3. Truncatated frequency profiles for triple junctions sampled between 70 and 105 degrees of angle. (**a**) calculated profile for 408,426 trial intersections (i.e., equivalent to one million trials for all angles between 0 and 180 degrees); (**b**) calculated profile for 305 trials (equivalent to 746 trial intersections between 0 and 180 degrees of angle); (**c**) measured 680 °C calibration profile (n = 305) for galena dihedral angles, θ_{gn}. The theoretical dihedral angle is 89 degrees in (**a**) and (**b**). The true angle in (**c**) is estimated to be 89 degrees based on iterative analysis. Compare the smooth cuspate form of the profile in (**a**) with the jagged profiles in (**b**) and (**c**) where the subsidary spikes have no statistical significance.

gives the correct value to an accuracy of one degree as determined by the standard deviation. About 300 of these angles can be discarded as obviously belonging to the extremes of the full range (i.e., 0 to 180 degrees). Thus, about 700 well-chosen measurements will remain. In practice, however, 300 measurements routinely take 16 to 18 hours (or 2 days). For unimodal populations of this size, the accuracy is reduced to about 2 degrees as assessed from the standard deviation. In one exceptional trial, the largest peak by a small margin was found to be displaced by 8 degrees from the true angle, leaving it skewed against the background peak. Where statistical anomalies of this kind occur, measurements can be continued until the side peak reduces. On the other hand, side peaks (or secondary modes) in natural sample profiles can be real, and will persist as more data are accumulated. Smoothing techniques using

$$a_j' = (a_{j+1} + 2a_j + a_{j-1})/4$$

(where a_j is the number of measurements in the j^{th} bin and a_j' is the new smoothed value) were tried with our model data sets. The results improved the standard deviations of our trials from about 1.5 to 1 degree. However no additional certainty is offered by these techniques where fewer than 300 measurements are involved. For the examples given in Figures 3b and 3c, the maximum peak heights occur fortuitously at 88 degrees. These deviate slightly from the set value of 89 degrees for the model data in Figures 3a and 3b, and the same angle obtained by the smoothing procedure for the real data indicated in Figure 3c.

Practical ranges for measurement were selected because the full 0–180 degree range is not needed. For samples where the most frequent angle can be anticipated to within 5 degrees, a range as small as 25 degrees is satisfactory. Ranges of measurement to 40 degrees were used where prior estimates were uncertain. This larger range was especially important for natural samples that were metamorphosed at high temperatures.

Interpreting measurement profiles for some natural samples can be difficult, and is necessarily subjective where more than one mode exists. After rejecting obviously anomalous (low and high) values, systematic trends that increase toward a principal mode from opposite sides can be identified. As was mentioned previously, an average accuracy of 2 degrees is anticipated for essentially unimodal populations of ~300 measurements. Where clearly defined modes are not evident in profiles due to localized flattening, arbitrarily centered θ values can be reported. However these values may not yield the best estimates of thermal events. It is therefore recommended that the range of flattening also be reported. These procedures have been followed in presenting the summary data for natural samples (see Table 3).

Most measurements were carried out routinely and yielded data with an average uncertainty within two degrees. However, the measurement of some dihedral angles must be approached with caution, or not attempted. Caution is required where significant plucking (due to polishing) along grain boundaries partly obscures contacts, and where obvious deformation effects are present near triple-junction locations. The measurement of dihedral angles defined by high curvature boundaries can be difficult, and should be avoided where it is likely to yield unreliable data. Figure 1b illustrates two situations where measurements should not be attempted. The first involves localized foreign mineral inclusions, however small, that occur at triple-junction locations. The second is a related situation that is relatively uncommon. In the example shown, a thin rim of a barely discernible Cu-Fe sulfide separates the pyrrhotite and sphalerite surfaces of the sphalerite-pyrrhotite-sphalerite triple-junction in the lower right of the figure. A final precaution to be observed is that X-Y tracking should be spaced sufficiently to prevent re-measuring the same angles. Advance planning can usefully facilitate the collection of separate data sets from localized areas within the same sample. Where significant differences in microfabric exist, a comparison of the profiles obtained from different areas can prove valuable in distinguishing between real and illusory (i.e., statistically anomalous) modes.

CALIBRATION RESULTS

Table 1 presents θ-T calibration data obtained from experiments carried out at 5 to 10 temperatures. The results for the θ_{sp}, θ_{po}, and θ_{gn} calibrations are plotted in Figure 4. The three calibration curves show that dihedral angles decrease smoothly, but more rapidly with increasing temperature. Thermometer sensitivity is therefore greatest at the highest temperatures, although the effect is less pronounced for the θ_{sp} calibration. For the latter calibration, it will be noted that the dihedral angle for sphalerite passes through 120 degrees near 1075 K (~800 °C), thus simulating the equilibrium condition for triple-junctions in single-phase aggregates.

The inset in Figure 4 shows the θ_{gn}-T data of Stanton and Gorman (1968). For temperatures between 575 and 1025 K, the agreement between θ_{gn} values for the two data sets is within one degree, and therefore excellent. However for temperatures between 1025 and 1225 K, the dashed curve of Stanton and Gorman (representing selected "best" data) is up to ~2.5 degrees lower than for θ_{gn} values in the present calibration.

A function was found that yields good fits to the calibration data sets and also provides satisfactory extrapolations to 0 K and T_c, where the computed values of T_c approach the respective melting temperatures for the calibration sulfides. The generic function is:

$$\theta(T) = A\{1 - \exp[B(T - T_c)]\}$$

where A, B, and T_c are constants, T and T_c are in Kelvin, and $\theta(T)$ is in degrees of angle. The fitting parameter, T_c (often called a critical temperature in equations of this form), is found to

TABLE 1. Dihedral angle vs. temperature calibrations

Experiments		Dihedral angles (degrees)		
time (days)	temp. (°C)	θ_{sp}	θ_{po}	θ_{gn}
375	282	n.d.	113.5	111
230	380	129	112	109
164	483	128	110.5	105.5
140	580	126.5	107.5	98
56	680	123	102.5	89
22	780	121	n.a.	76.5
51	880	117.5	n.a.	58
14	925	n.d.	n.a.	47.5
14	951	n.d.	n.a.	37
3	980	112	n.a.	23

Notes: n.d. = not determined; n.a. = not available.

approximate the melting temperature. The following equations were derived for the three calibrations:

$$\theta_{sp}(T) = 129.9\{1 - \exp[0.00425(T\text{-}1709)]\}$$
$$\theta_{po}(T) = 116.5\{1 - \exp[0.00425(T\text{-}1450)]\}$$
$$\theta_{gn}(T) = 115.5\{1 - \exp[0.00425(T\text{-}1313)]\}$$

All $\theta(T)$ values reduce rapidly to zero near the T_c values. The T_c values obtained for pyrrhotite and galena agree to within 0.5% of the eutectic melting temperatures for pyrrhotite (~1443 K; Kullerud 1966) and galena (~1318 K; Kullerud 1966). We also point out that the same value has been used for B in each case (i.e., 0.00425 per K). This common value is justified because the values obtained independently agreed to within 1%, and there were no significant changes in the least-squares error sums when the common value was substituted. As our fitting procedures give curves that include all of the experimental points to within the statistical error of two degrees, we anticipate that these equations have general application for sulfides and that the extrapolations to higher temperatures can be used with reasonable confidence. The equations above were used to generate the smoothed data that is presented in Table 2.

The smoothed data given in Table 2 can be combined with the equations $\lambda_{gn-gn} = 2\lambda_{sp-gn} \cos(\theta_{sp}/2)$ and $\lambda_{sp-sp} = \lambda_{gn-sp} \cos(\theta_{gn}/2)$, which define equilibrium conditions for true dihedral angles of respective triple junctions at chosen temperatures. The relative surface energy ratios, $\lambda_{gn-gn}/\lambda_{sp-sp}$, involving galena ($\lambda_{gn-gn}$) and sphalerite ($\lambda_{sp-sp}$) surface tensions, are thus obtained as a function of increasing temperature. These ratios for shared galena vs. shared sphalerite grain boundaries decrease non-linearly from ~0.79 at 0 K to ~0.57 at 1220 K.

APPLICATION TO NATURAL SAMPLES

The $\theta_{gn}(T)$ calibration has been applied to sphalerite-galena assemblages in selected ore samples for which independent and apparently reliable estimates of temperature are available. The $\theta_{po}(T)$ calibration also has been applied to three of the same samples that contained sufficient pyrrhotite for analysis. Table 3 presents summary TJT data for six sulfide deposits that are listed in order of increasing regional metamorphic grade (i.e., from sub-/low greenschist to granulite facies).

A selection of microfabrics found in the ores investigated here is shown in Figures 5a–h. The photomicrographs in this figure are assembled in order of increasing regional metamorphic grade. All of the ores contain major sphalerite, major to minor amounts of galena, and minor amounts of chalcopyrite

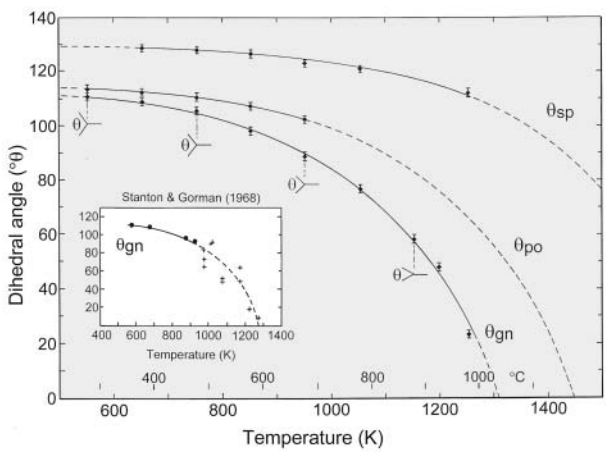

FIGURE 4. Calibrations of dihedral angles for sphalerite (θ_{sp}), pyrrhotite (θ_{po}) and galena (θ_{gn}) vs. temperature (K). The inset shows the $_{gn}$- T data of Stanton and Gorman (1968).

TABLE 2. Smoothed data for temperature vs. dihedral angles, θ (T)

T (°C)	T(K)	θ, (degrees)		
		θ_{sp}	θ_{po}	θ_{gn}
	0	(129.808)	(116.252)	(115.061)
177	450	(129.279)	(114.828)	(112.536)
277	550	(128.951)	113.944	110.968
377	650	128.449	112.593	108.573
477	750	127.682	110.528	104.910
577	850	126.509	107.371	99.312
677	950	124.716	102.544	90.753
777	1050	121.975	(95.166)	77.670
877	1150	117.786	(83.888)	57.671
927	1200	(114.922)	(76.178)	44.000
977	1250	111.382	(66.646)	27.098
1027	1300	(107.004)	(54.861)	(6.200)
1040	1313	(105.705)	(51.365)	(0.000)
1077	1350	(101.591)	(40.290)	
1127	1400	(94.899)	(22.274)	
1177	1450	(86.625)	(0.000)	
1227	1500	(76.395)		
1277	1550	(63.747)		
1327	1600	(48.109)		
1377	1650	(28.774)		
1427	1700	(4.868)		
1436	1709	(0.000)		

Note: Parentheses contain interpolated values derived from equations given in the text.

TABLE 3. Summary TJT results for massive sulfide deposits

Deposit	no. meas.	max. $^1\theta_{gn}$, $^2\theta_{po}$	estim. temp.(°C)	metam. grade
Cobar (CSA)	325	^{1}110.5	~280	sub-low
(N.S.W.)	330	^{2}114	~260	grn./ sch.
Woodlawn	322	^{1}109	~370	low grn.
(N.S.W.)				/ sch.
SWBD (N.B.)	300	^{1}105	~480	mod. grn.
		^{1}110(R)	~300(R)	/ sch.
BM&S, no. 12 (N.B.)				
no. 425	367	^{1}106	~470	mod. grn. / sch.
no. 575	320	^{1}105	~480	
		^{1}111(R)	~240(R)	
Ruttan (Man.)	369	^{1}97	~590	low
		^{2}110~500 or (107–113)	(~590–340)	amphib.
Broken Hill (N.S.W.)				
no. 4	463	^{1}~91 or (~87–93)	~650 (~690–630)	granulite
		^{1}100		~550(R)
		^{2}101.5	~690	
		^{2}106.5?	~600	
no. 7	470	^{1}~90 or (~85–95)	~660 (~710–610)	granulite
		^{1}101		~540(R)

Note: (R) = proposed recrystallization.

and/or cubanite. Several also contain major to minor proportions of pyrrhotite. Pyrite does not occur in the Broken Hill or Cobar samples, but occurs as a major phase in the other samples.

Cobar and Woodlawn ores (N.S.W., Australia)

The Zn- and Pb-rich sample of massive Cobar ore that was used in the calibration experiments was strongly foliated and

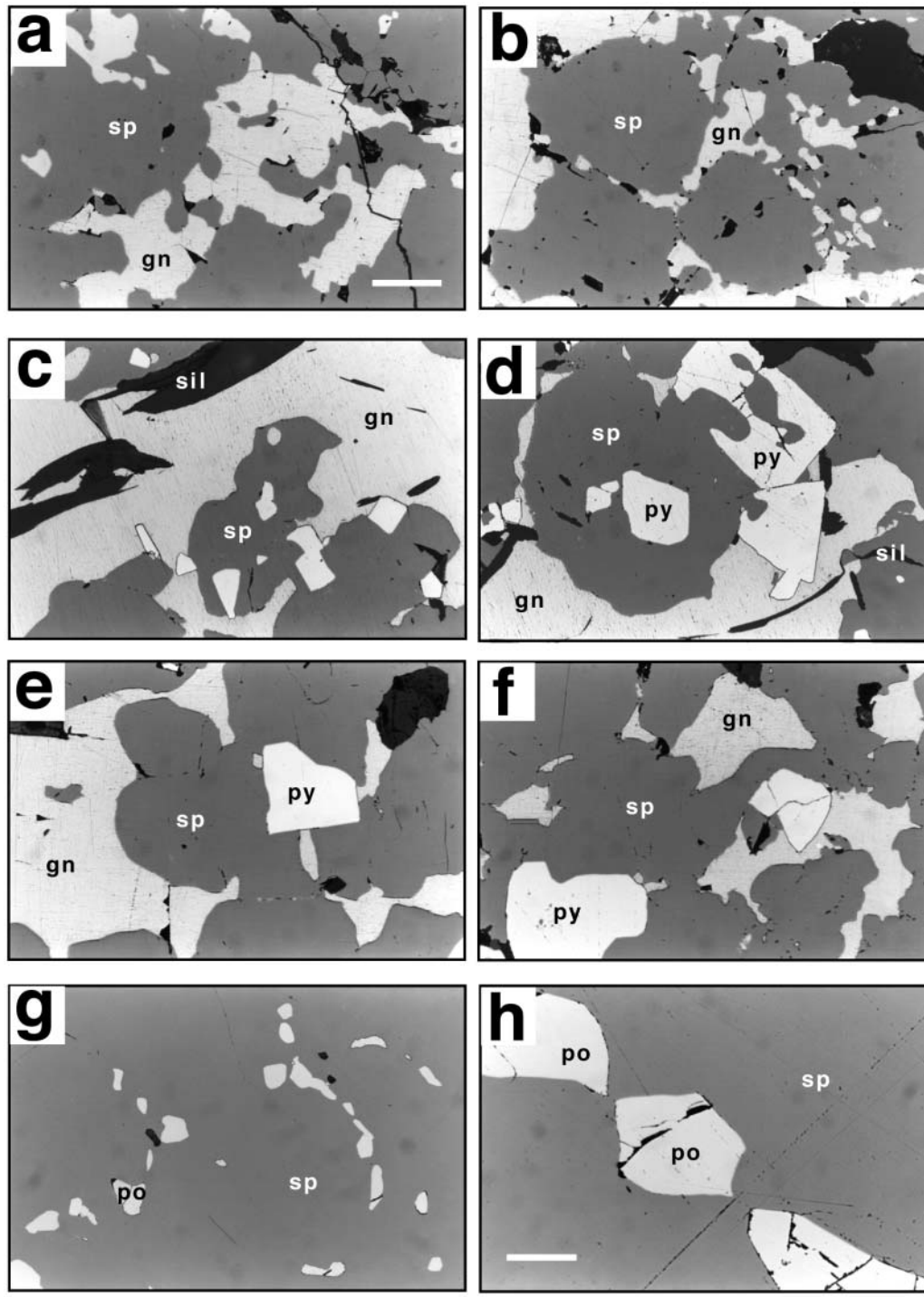

FIGURE 5. Photomicrographs of: (**a**,**b**) annealed fabrics in the Cobar ore sample; (**c**,**d**) sulfides and deformed silicates (sil) in the Woodlawn ore; (**e**,**f**) relatively undeformed (**e**) and deformed (**f**) sphalerite-galena intergrowths in the SWBD sample; (**g**) pyrrhotite-sphalerite "net" textures in the Ruttan ore; (**h**) pyrrhotite-sphalerite intergrowths in Broken Hill sample no. 4. All photomicrographs are at the same scale with the bars representing 100 micrometers.

generally fine grained. However, under the microscope it exhibits an essentially annealed microfabric (Figs. 5a and 5b). This implies that a thermal event followed an earlier major deformation(s). These observations are consistent with precursor sedimentary sulfides that were strongly deformed and later annealed at sub- to low greenschist facies regional metamorphic conditions. On the other hand, a syn-metamorphic, hydrothermal origin is evident for some sulfide ores in the Cobar area (de Roo 1989; Seccombe 1990).

Heating experiments at ≥380 °C have changed dihedral angles in the Cobar sample and yielded good θ_{sp}, θ_{gn}, and θ_{po} calibration data. However, in the lowest temperature heating experiment (~280 °C), no changes in θ_{gn} or θ_{po} dihedral angles were detected. It can be concluded, therefore, that the natural microfabric in the Cobar sample is compatible with a maximum metamorphic temperature of ~280 °C, although the uncertainty of estimate is at least 100 °C. θ_{gn} and θ_{po} profiles for the natural Cobar sample are shown in Figures 6a and 6b.

Allowing for the large degree of temperature uncertainty associated with the calibrations at low temperatures, both TJT values compare reasonably with independently determined temperatures. Brill (1988), in determining a regional pressure of ~3 kbar using illite crystallinity, reported fluid inclusion homogenization (minimum) temperatures of 240–370 °C (~300 °C average) for metamorphic quartz and chlorite at the C.S.A. Mine. At the neighboring Elura Mine, Seccombe (1990) obtained a 300 to 365 °C range in homogenization temperatures for quartz, and a 335 to 200 °C spread of sulfur isotope temperatures for sphalerite-galena pairs. Seccombe (1990) attributed the lower temperatures to recrystallization effects.

The volcanogenic Woodlawn deposit has been regionally metamorphosed at the low greenschist facies (Gilligan et al. 1979). For the single sample analyzed, a θ_{gn} dihedral angle of ~109 degrees was obtained (Fig. 7). This value equates to a calibration temperature of approximately 370°. The latter shows excellent agreement with higher sulfur isotopic temperature data obtained by Ayres et al. (1987) for four sphalerite-galena pairs (350–400 °C; averaging 360 ± 30 °C). Another group of samples with isotopic temperatures between 225 and 300 °C is presently reinterpreted to indicate retrograde recrystallizations. Lusk and Krouse (1997) reported homogenization (minimum) temperatures (~150 – ~350 °C) for fluid inclusions in quartz that overlap with the sulfur isotopic temperatures.

Bathurst Camp ores (New Brunswick, Canada)

Three samples were chosen for study, including two widely separated samples from the B.M. and S. no. 12 deposit and one from the South West Boundary deposit (SWBD). Lusk and Krouse (1997) described sample no. 425 (sample 1, Table 1) and no. 575 (sample 2, Table 1) from the no. 12 deposit in an earlier isotope and fluid inclusion study. All of these samples exhibit deformational features that have resulted from complex folding (de Roo et al. 1991; Lentz and van Staal 1995), and thermal effects due to moderate greenschist-facies (biotite zone) regional metamorphism. The *T-P* conditions of regional metamorphism correspond to a suggested temperature of ~450 °C (Lusk and Krouse 1997), and a regional pressure of ~4–6 kbars (Lentz and Goodfellow 1993).

Profiles for galena dihedral angles, θ_{gn}, in the no. 425 and no. 575 samples are presented in Figure 8 and profiles for the SWBD sample are shown in Figure 9. The principal modes are tightly constrained within the narrow range of 105 to 106 degrees. The latter equate with calibration temperatures of 470–480 °C, for which the respective estimate of error is ~ ± 70 °C. These triple-junction temperatures compare favorably with metamorphic fluid inclusion boiling temperatures to 440 °C reported for the no. 425 sample and in two other widely separated samples from the no. 12 deposit (Lusk and Krouse 1997).

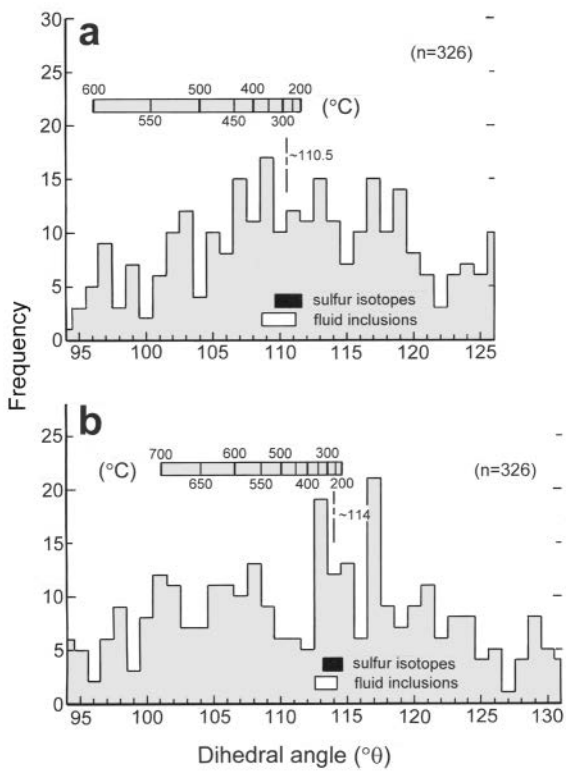

FIGURE 6. Dihedral angle profiles for (**a**) galena, θ_{gn}, and (**b**) pyrrhotite, θ_{po}, in the untreated Cobar ore, N.S.W., Australia.

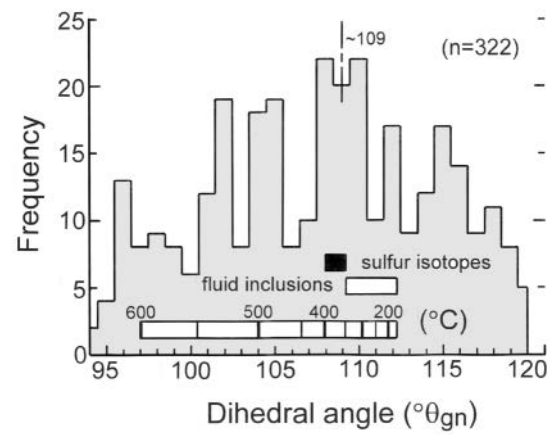

FIGURE 7. Dihedral angle profile for galena, θ_{gn}, in the Woodlawn ore from N.S.W.

Temperatures between 435 and 355 °C ($\sigma = \pm 35$°C) were obtained from sulfur isotopes in the no. 425 and no. 575 samples. Lusk and Krouse (1997) interpreted these lower temperatures to indicate deformation-induced recrystallization effects that occurred on the microscale during retrograde cooling.

Localized recrystallization effects can be anticipated also in the θ_{gn} data. Indeed, such an effect may be present in the no. 575 profile around 111 degrees where a secondary mode is suggested. The latter corresponds to a temperature of ~240 °C. This temperature overlaps with an episode of enhanced fluid activity (i.e., ~230 and ~330 °C) that was reported by Lusk and Krouse (1997) for fluid inclusion homogenization temperatures.

The θ_{gn} data for the SWBD sample were collected from three separate areas on a ~30 × ~25 mm polished surface, as shown in the inset of Figure 9a. The profiles for each of the populations of ~100 measurements shown in Figures 9b–d reveal differences that were correlated with subjective visual observations. For example, it was noted that the C area appeared to be the most deformed texturally, as was judged from local concentrations of fractures, and by the waviness or displacements in shared sphalerite-galena grain boundaries (e.g., Fig. 5f). The matching θ_{gn} profile suggests a mode around 110 degrees. The A and B areas suggested considerable deformation in parts only (e.g., Fig. 5e). The A area profile indicates two distinct modes, with the principal mode located around ~105 degrees and a secondary mode around ~110 degrees. The B area profile appears to be transitional between the A and C profiles. The profile for the aggregated data (Fig. 9a) yields a distinct principal mode around ~106 degrees (~470 °C) and a genuine secondary mode around ~110 degrees (~300 °C). It can be noted from Figure 9a that the sulfur isotopic temperatures (i.e., 325, 355, and 405 °C) occur between the two modes, but appear closest to the secondary mode at ~110 degrees. This implies that the sulfur isotopic temperatures were strongly influenced by the retrograde recrystallization that produced the secondary mode around 300 °C.

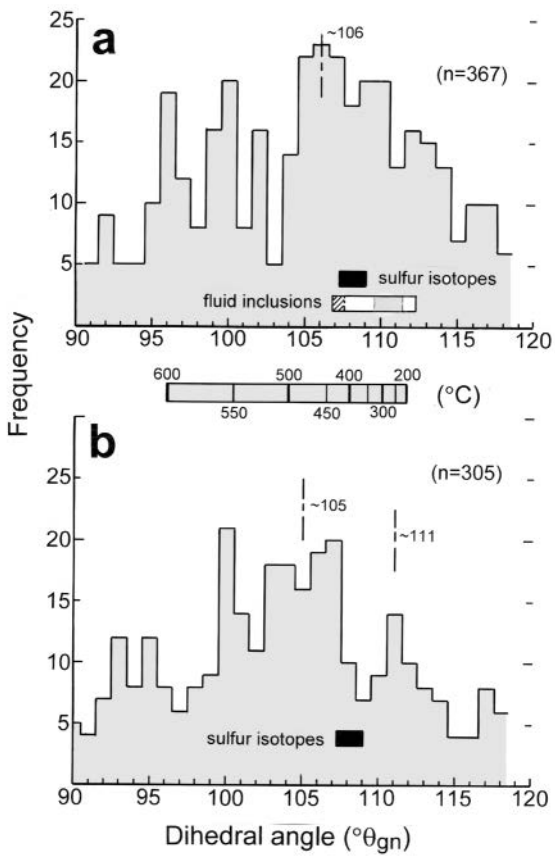

FIGURE 8. Dihedral angle profiles for galena, θ_{gn}, in the (**a**) no. 425 and (**b**) no. 575 samples from the B.M.& S. no. 12 deposit, N.B., Canada.

Ruttan ore (Manitoba, Canada)

The dihedral angles for galena and pyrrhotite were measured in a single sample of pyrite- and sphalerite-rich ore containing minor amounts of galena and pyrrhotite. The relatively coarse-grained pyrite porphyroblasts in this sample tend toward rectangular outlines in section and show a general alignment or lineation. The minor proportions of galena are concentrated locally, and its shared boundaries with sphalerite suggest appreciable deformation. The minor pyrrhotite appears to be more evenly distributed throughout the abundant sphaler-

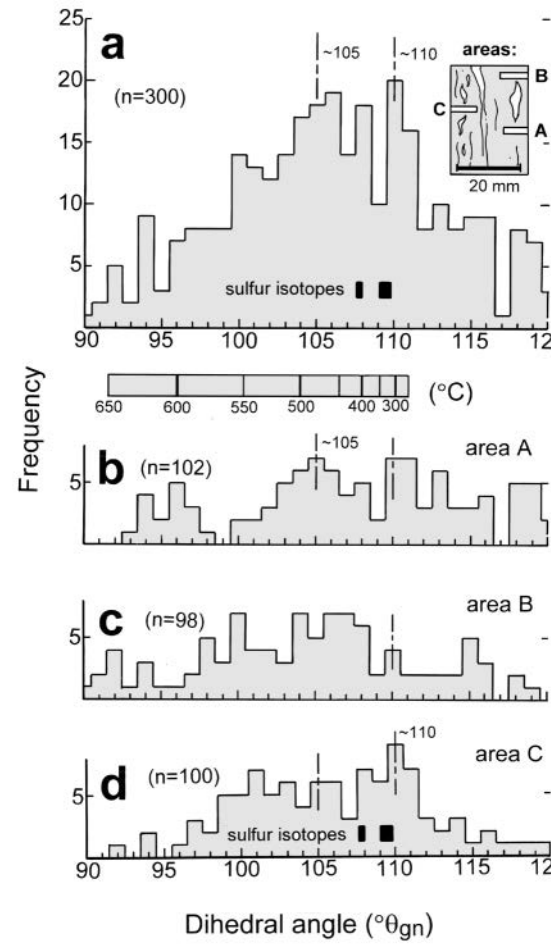

FIGURE 9. (**a**) Aggregate θ_{gn} data for the SWBD sample, Bathurst Camp, New Brunswick; (**b**-**d**) dihedral angle profiles ($n \sim 100$) for galena, θ_{gn}, in Areas A, B, and C shown in the inset a.

ite, and its generally smooth boundaries with sphalerite suggest a lower degree of superimposed deformation. Much of the pyrrhotite is located along shared grain boundaries in the relatively coarse-grained sphalerite resulting in net-like textures (e.g., Fig. 5g).

Profiles of the dihedral angles for galena and pyrrhotite are presented in Figure 10. The dihedral angles for galena, θ_{gn}, yield an unusually low profile with numerous spikes. The latter apparently reflect the considerable degree of deformation that is present in this randomly selected sample. Bearing in mind the high level of uncertainty in interpreting the galena results, a provisional "primary" mode is estimated to occur around 97 degrees (~590 °C). By way of contrast, the θ_{po} profile is smoother overall, but lacks a definitive primary mode in the interval where grouped frequencies are highest [i.e., 107 (~590 °C) to 113 (~340 °C), with a median at ~110 (~500 °C) degrees]. However, the lowest group frequency value of 107 degrees corresponds to a temperature of ~590 °C, and this temperature is shared by the provisional θ_{gn} peak (i.e., 97 degrees) value.

Sulfur isotopic temperatures were obtained from two adjacent volumes (~1.5 cm^3) in the same ~70 mm hand specimen on which the TJT analyses were performed. Lusk and Krouse (1997) reported the results for bulk isotopic analyses on the sulfide separates from these sample volumes. One sample yielded a reasonably tight grouping of temperatures at 430, 440, and 405 °C for pyrite-sphalerite, sphalerite-galena, and pyrite-galena pairs, respectively. The second sample gave temperatures of 310, 480, and 385 °C for respective pairs, thus indicating wider temperature variation and apparent departures from isotopic equilibrium (Fig. 10). These are obviously recrystallization effects that overlap with possible secondary modes at around 109 degrees (~350 °C) for the θ_{gn} thermometer, and at ~113 degrees (~340 °C) for the θ_{po} thermometer. The pyrrhotite "net" texture within sphalerite (Fig. 4g) may have developed at the maximum metamorphic temperature. However, if a descending *P-T* path was followed during retrograde cooling, some of the pyrrhotite could have been resorbed by its sphalerite host (cf., Scott 1973), and the "net" texture partially reset during the lower temperature recrystallization(s). Although the ~590 °C θ_{gn} maximum for the metamorphism is speculative, it falls within the 550 to 650 °C (and at pressure of ~5 kbars) range that was reported by Bristol (1979) for metamorphic silicates associated with the Ruttan deposit.

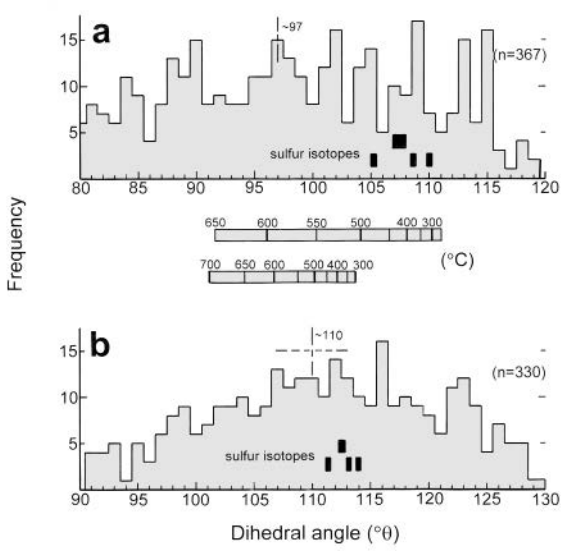

FIGURE 10. Dihedral angle profiles for (**a**) galena, θ_{gn}, and (**b**) pyrrhotite, θ_{po}, in an ore sample from the Ruttan deposit, MAN., Canada.

Broken Hill ores (N.S.W., Australia)

Study was undertaken on two widely separated samples of Broken Hill ore containing ~55% of Fe-rich sphalerite and ~30% galena, together with minor amounts of pyrrhotite and silicates. Careful inspection revealed apparent uniformity in the macrofabrics and also in the grain sizes that were estimated to average around 4–5 mm. The ores have been subjected to granulite-facies regional metamorphism for which Phillips (1980) reported a peak temperature of ~780 °C based on silicate thermometry. Estimates of pressure range from 5.2 ± 0.3 (Phillips 1980) to 6.8 ± 0.3 kbars (Bryndzia et al. 1988).

The results of θ_{gn} and θ_{po} measurements made on sample no. 4 are presented in Figure 11. Dihedral angle measurements for galena in sample no. 7 are shown in Figure 12. Truncated θ_{gn} results, spanning 65 degrees of measurement (i.e., 55 to 120), are shown as split histograms. The θ_{gn} histogram for sample no. 4 (Fig. 11a-b) suggests a provisional principal mode at ~91 degrees (~660 °C) and a possible secondary mode at ~100.5 degrees (~550 °C). The split θ_{gn} profile for sample no. 7 (Fig. 12) also shows a well-defined mode at ~101 degrees (~540 °C), and a possible second mode at ~95 degrees (~620 °C). However, the latter forms part of a broad region of higher frequencies occurring between 95 and 85 degrees (~710 °C), for which a centered value of ~90 degrees (~660 °C) is arbitrarily indicated. Figure 11c shows the θ_{po} profile obtained for sample no. 4. Two distinct modes are indicated, including one at ~101.5 degrees (~690 °C; established through sub-area analysis) and the other at ~106.5 degrees (~600 °C). After considering all of the TJT data for the Broken Hill samples, a shared maximum metamorphic temperature of ~700 °C is suggested, together with apparent recrystallization effects ranging from ~630 down to at least ~540 °C.

The ~700 to ~540 °C temperature range inferred from the triple-junction thermometers brackets the sulfur isotopic temperatures obtained from sphalerite-galena pairs. Sulfur isotopic temperatures of 560 ± 55, 600 ± 55, and 670° ± 60 °C were obtained from duplicate analyses made on sphalerite and galena concentrates prepared from each of three 10 mm cubes cut from sample no. 4 (60 mm hand specimen). Two similarly prepared and treated cubes from sample no. 7 yielded sulfur isotopic temperatures of 630 ± 50 and 680 °C (single analyses). Thus sulfur isotope thermometry implies a 120 °C spread of temperatures that appears to be real. These data, together with the TJT results, demonstrate the occurrence of localized domains of recrystallization(s) that were present in the cubes and also in the polished sample blocks on which the TJT measurements were made. Elsewhere in the deposit, even lower temperature recrystallization events (i.e., ~540 to ~300 °C) are

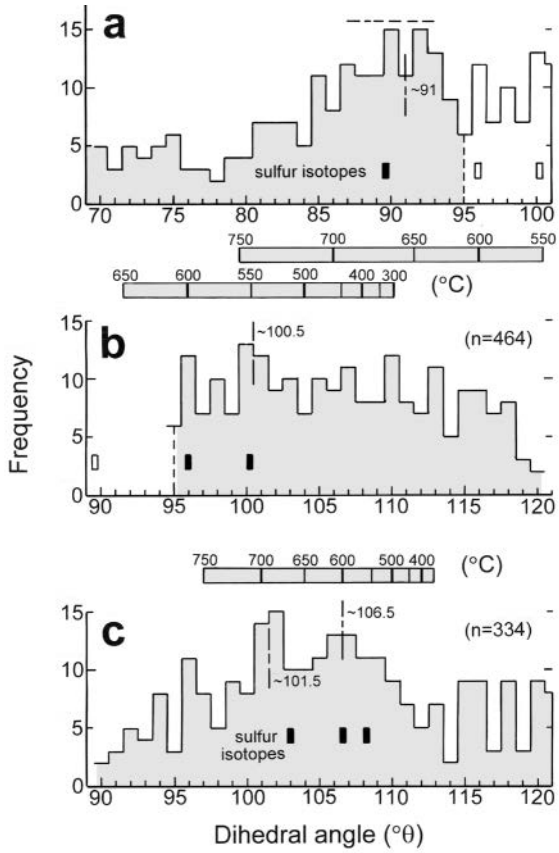

FIGURE 11. Dihedral angle profiles for (**a**-**b**) galena, θ_{gn}, and (**c**) pyrrhotite, θ_{po}, in sample no. 4 from Broken Hill, N.S.W., Australia.

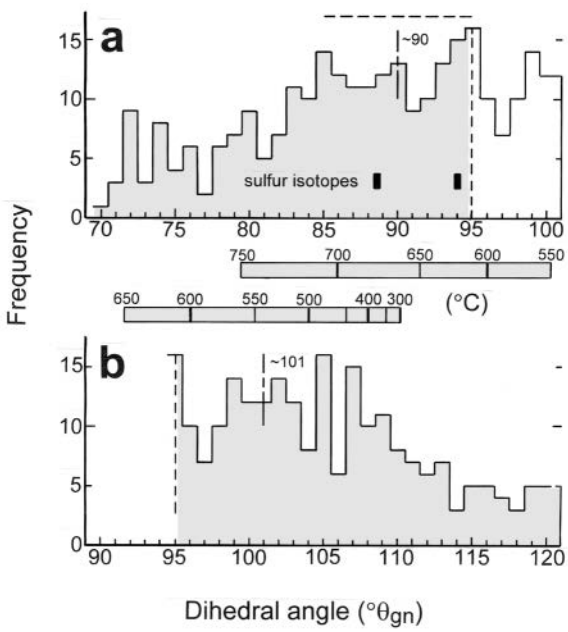

FIGURE 12. Dihedral angle profile for galena, θ_{gn}, in sample no. 7 from Broken Hill.

implied from sulfur isotope thermometry (Stanton and Rafter 1967; Both and Smith 1975). Additionally, an independent fluid inclusion study by Wilkins (1977) showed that repeated deformation and recrystallization involving a sequence of fluids had occurred during retrograde cooling of this deposit.

CONCLUDING REMARKS

This first application of the θ_{gn} and θ_{po} triple-junction thermometers to a selection of regionally metamorphosed massive sulfide ores demonstrates that natural fabrics achieved conditions of physical equilibrium that reflect the maximum temperatures of their respective metamorphisms. These conditions include the attainment of equilibrium grain size in addition to matching dihedral angle relationships, both of which are temperature-dependent. Larger grain size equates in turn with larger radii of curvature for shared surfaces between grains, and with net reductions of both surface free energy and shared surface areas per unit volume (Ewers 1967). The apparent retention of physical equilibrium properties corresponding to maximum metamorphic temperatures implies that the activation energies required for grain-size reduction and for dihedral angle adjustments are not achieved during retrograde cooling, unless deformation-induced recrystallization has occurred. The present study suggests that recrystallization effects can be expected in all regionally metamorphosed sulfide ores.

Combining sulfur isotope with triple-junction thermometry has been essential to the present study on massive sulfide ores. The two methods are complementary in that isotopes are most sensitive at the lowest temperatures whereas the triple-junction thermometers are most sensitive at the highest temperatures. These thermometers are also radically different in their methodologies and in the information that they provide. Triple-junction thermometry involves grain-by-grain analysis, and the capacity to reveal separate thermal events, such as peak regional metamorphic temperatures and subsequent major deformation-induced recrystallization(s). This capacity has been demonstrated for the SWBD (New Brunswick) and Broken Hill (N.S.W.) ores. On the other hand, sulfur isotope thermometry using the bulk analysis method can yield reliable equilibrium recrystallization temperatures, or combine the effects of any real differences to yield weighted (and non-equilibrium) estimates of temperature. These claims were made by Lusk and Krouse (1997), who reported that a range of equilibrium sulfur isotopic temperatures can be obtained from spatially separated samples within a given massive sulfide deposit, and also that temperature variations can be indicated between small sample volumes from single hand specimens. The present TJT study provides textural and thermal confirmation of these claims. Hence, lower sulfur isotopic temperatures must be recognized for what they are, namely, the products of localized recrystallization(s) that occurred during retrograde cooling.

Sulfur isotope thermometry employing microanalysis techniques with improved precision (cf., Valley et al. 1998) may be developed in the future. Nevertheless, it will be necessary to carry out many analyses on coexisting mineral pairs in single samples in order to yield equivalent thermal information that is provided by the TJT method.

The present study highlights the importance of recognizing

deformation effects that are present in the microfabrics of all regionally metamorphosed ores. These effects include microfractures and displacements, openings along grain boundaries and cleavage planes, and stepwise cleavage-controlled displacements of galena-sphalerite boundaries. Some of the latter features are sharply defined and therefore appear to be younger, whereas others appear to have been annealed, or partly annealed, to yield rounded or wavy boundaries. Deformation features are typically localized, and their intensity can vary greatly over short distances. It is therefore important to recognize deformation features and not, for example, to attempt erroneous angular measurements on cleavage-controlled displacements. The adoption of a sound measurement strategy involving measurement in sub-areas, combined with careful textural observation, is strongly recommended.

Triple-junction thermometry is simple, non-destructive, and inexpensive to apply. The method also offers unique properties and advantages. An inherent property of the method is the inter-dependence of thermal signatures and metamorphic microfabrics. TJT can thus reveal information that hitherto has been overlooked in conventional geothermometry studies. A second property of the method is that chemical reaction between participating mineral species is not a prerequisite, in contrast with isotope and other types of mineralogical thermometers. The triple-junction method of thermometry will therefore be applicable to any combination of regional metamorphic minerals (e.g., oxides, sulfides, carbonates, silicates, etc.), provided relative differences in surface tensions are appropriate for obtaining usable calibration curves similar to those employed in the present study. Chosen pairs also require wide ranges of *P-T* stability.

This new method of thermometry offers previously unrealized opportunities. However, there are a number of questions that will need to be addressed in subsequent studies. Although the TJT method is physically based, large degrees of compositional variation within specific minerals will affect surface tensions, and potentially calibrations. However, the present experience with natural sphalerites showing ~25 mol% variation (i.e., ~10 to ~35 mol%) in FeS content suggests that such effects could be relatively unimportant. High confining pressures may also have an effect on TJT thermometers, but the effect is likely to be minor due to the relatively low compressibilities of minerals, even at the higher temperatures and pressures within the crust.

ACKNOWLEDGMENTS

The authors thank C. Cooper in the Department of Mathematics, Division of Mathematics, Computing, Physics, and Electronics, Macquarie University, for advice and assistance. D.W. Durney and staff of the Department of Physical Geography are thanked for making available laboratory facilities that have enabled us to complete this project. The skilful assistance of P. Zeller in customizing a microscope and that of T. Bradley in preparing some of the polished mounts is gratefully acknowledged. Funding was provided by the Macquarie University Research Grants Scheme.

REFERENCES CITED

Ayres, D.E., Burns, M.S., and Smith, J.W. (1987) Sulfur isotope study of the massive sulfide orebody at Woodlawn, New South Wales. Journal of the Geological Society of Australia, 26, 197–201.

Both, R.A. and Smith, J.W. (1975) A sulfur isotope study of base metal mineralization in the Willyama Complex, Western New South Wales, Australia. Economic Geology, 70, 308–318.

Brill, B.A. (1988) Illite crystallinity, b_o and Si content of K-white mica as indicators of metamorphic conditions in low grade metamorphic rocks at Cobar, N.S.W., Australia. The Australian Journal of Earth Sciences, 35, 295–302.

Bristol, C.C. (1979) Application of sphalerite geobarometry to ores from the Ruttan Mine. Economic Geology, 74, 1496–1502.

Bristol, L.T., Scott, S.D., and Spry, P.G. (1988) Sphalerite and hexagonal pyrrhotite geobarometer: Experimental calibration and application to the metamorphosed sulfide ores of Broken Hill, Australia. Economic Geology, 83, 1193–1204.

Bristol, W.E. (1967) Physico-chemical aspects of recrystallization. Mineralium Deposita, 2, 221–227.

de Roo, J.A. (1989) The Elura Ag-Pb-Zn mine in Australia-ore genesis in a slate belt by syndeformational metasomatism along hydrothermal fluid conduits. Economic Geology, 84, 256–278.

de Roo, J.A., Williams, P.F., and Moreton, C. (1991) Structure and evolution of the Heath Steele base metal orebodies, Bathurst Camp, New Brunswick, Canada. Economic Geology, 86, 927–943.

Gilligan, L.B., Felton, E.A., and Olgers, F. (1979) The regional setting of the Woodlawn deposit. Geological Society of Australia, 26, 135–140.

Kullerud, G. (1966) Phase relations in sulfide-type systems. In Clark Jr. S.P., Ed., Handbook of physical constants (rev. ed.), Memoir 97, 14, 325–342. Geological Society of America, Inc. New York.

Lentz, D.R. and Goodfellow, W.D. (1993) Petrology and mass-balance constraints on the origin of quartz-augen schist associated with the Brunswick massive sulfide deposits, Bathurst, New Brunswick. The Canadian Mineralogist, 31, 877–903.

Lentz, D.R. and van Staal, C.R. (1995) Predeformational origin of massive sulfide mineralization and associated footwall alteration at the Brunswick 12 Pb-Zn-Cu deposit, Bathurst, New Brunswick: Evidence from the porphyry dike. Economic Geology, 90, 453–463.

Lusk, J. and Krouse, H.R. (1997) Comparative stable isotope and temperature investigation of minerals and associated fluids in two regionally metamorphosed (Kuroko-type) volcanogenic massive sulfide deposits. Chemical Geology, 143, 231–253.

Ohmoto, H. (1986) Stable isotope geochemistry of ore deposits. In Valley, J.W. et al., Eds., Stable isotopes in high temperature processes, 16, 491–559. Reviews in Mineralogy, Mineralogical Society of America, Washington, D.C.

Phillips, G.N. (1980) Water activity changes across the amphibolite-granulite facies transition, Broken Hill, Australia. Contributions to Mineralogy and Petrology, 75, 377–386.

Roedder, E. (1986) Fluid Inclusions. In Ribbe, P.H., Ed., 12, 1–644. Reviews in Mineralogy, Mineralogical Society of America, Washington, D.C.

Scott, S.D. (1973) Experimental calibration of the sphalerite geobarometer. Economic Geology, 68, 466–474.

Seccombe, P.K. (1990) Fluid inclusions and sulfur isotope evidence for syntectonic mineralization at the Elura Mine, southeastern Australia. Mineralium Deposita, 25, 304–312.

Sharp, Z.D., Essene, E.J., and Kelly, W.C. (1985) A re-examination of the arsenopyrite geothermometer: Pressure considerations and applications to natural assemblages. Canadian Mineralogist, 23, 517–534.

Smith, C.S. (1950) Interphase interfaces. Imperfections in nearly perfect crystals. Wiley, New York.

———(1964) Some elementary principles of polycrystalline microstructure. Metallurgical Reviews, 9, 1–48.

Stanton, R.L. (1955) Lower Palaeozoic mineralization near Bathurst, New South Wales. Economic Geology, 50, 681–714.

——(1964) Textures in stratiform ores. Nature, 202, 173–174.

Stanton, R.L. and Gorman, H.A. (1968) A phenomenological study of grain boundary migration in some common sulfides. Economic Geology, 63, 907–923.

Stanton, R.L. and Gorman Willey, H.A. (1970) Natural work hardening in galena, and its experimental reduction. Economic Geology, 65, 182–194.

Stanton, R.L. and Rafter, A.T. (1967) Sulfur isotope ratios in coexisting galena and sphalerite from Broken Hill, New South Wales. Economic Geology, 62, 1088–1091.

Valley, J.W. (1986) Stable isotope geochemistry of metamorphic rocks. In Valley, J.W., et al., Eds., Stable isotopes in high temperature processes, 13, 445–489. Reviews in Mineralogy, Mineralogical Society of America, Washington, D.C.

Valley, J.W., Graham, C.M., Harte, B., Eiler, J.M., and Kinny, P.D. (1998) Ion microprobe analysis of oxygen, carbon and hydrogen isotope ratios. In McKibben, M.A., Shanks III, W.C. and Ridley, W.I., Eds., Applications of microanalytical techniques to understanding mineralizing processes, 7, p. 73–98. Society of Economic Geology Reviews, Economic Geology.

Wilkins, R.T.W. (1977) Fluid inclusion assemblages of the stratiform Broken Hill ore deposit, New South Wales, Australia. Science, 198, 185–187.

MANUSCRIPT RECEIVED OCTOBER 6, 2001
MANUSCRIPT ACCEPTED JUNE 2, 2002
MANUSCRIPT HANDLED BY GRAY E. BEBOUT